Non-linear control of a hydraulic piezo-valve using a generalized Prandtl-Ishlinskii hysteresis model

Frederik Stefanski, Bartosz Minorowicz[a]
Johan Persson, Andrew Plummer, Chris Bowen[b]

[a]Faculty of Mechanical Engineering and Management, Institute of Mechanical Technology, Poznan University of Technology, Piotrowo Street 3, Poznan 60-965, Poland
[b]Centre for Power Transmission and motion Control, Department of Mechanical Engineering, University of Bath, Bath, BA2 7AY, UK

email: frederik.stefanski@gmail.com; bartosz.minorowicz@put.poznan.pl;
L.J.Persson@bath.ac.uk; A.R.Plummer@bath.ac.uk, C.R.Bowen@bath.ac.uk

Corresponding author:
Frederik Stefanski, email: frederik.stefanski@gmail.com, address: Faculty of Mechanical Engineering and Management, Institute of Mechanical Technology, Poznan University of Technology, Piotrowo Street 3, Poznan 60-965, Poland

Abstract

The potential to actuate proportional flow control valves using piezoelectric ceramics or other smart materials has been investigated for a number of years. Although performance advantages compared to electromagnetic actuation have been demonstrated, a major obstacle has proven to be ferroelectric hysteresis, which is typically 20% for a piezoelectric actuator. In this paper, a detailed study of valve control methods incorporating hysteresis compensation is made for the first time. Experimental results are obtained from a novel spool valve actuated by a multi-layer piezoelectric ring bender. A generalized Prandtl-Ishlinskii model, fitted to experimental training data from the prototype valve, is used to model hysteresis empirically. This form of model is analytically invertible and is used to compensate for hysteresis in the prototype valve both open loop, and in several configurations of closed loop real time control system. The closed loop control configurations use PID (Proportional Integral Derivative) control with either the inverse hysteresis model in the forward path or in a command feedforward path. Performance is compared to both open and closed loop control without hysteresis compensation via step and frequency response results. Results show a significant improvement in accuracy and dynamic performance using hysteresis compensation in open loop, but where valve position feedback is available for closed loop control the improvements are smaller, and so conventional PID control may well be sufficient. It is concluded that the ability to combine state-of-the-art multi-layer piezoelectric bending actuators with either sophisticated hysteresis compensation or closed loop control provides a route for the creation of a new generation of high performance piezoelectric valves.

Keywords

Hydraulic valve, piezoelectric actuator, non-linear control, hysteresis, Generalized Prandtl–Ishlinskii model

1. Introduction

Actuation using smart materials, such as piezoelectric ceramics and shape memory alloys, is an alternative to classical designs where movement is achieved by an electromagnetic force. Solenoids and torque motors are conventionally used in electrohydraulics to control flow and pressure. However, in the last two decades a number of new concepts which use smart materials have been described in literature [1,2]. The main aim of the application of smart materials has been to improve performance in terms of speed of response or accuracy, or to reduce mass or power consumption. In this paper, we describe a small spool valve actuated by a piezoelectric ring bender. The motivation for designing a piezoelectric actuated valve [3] is to avoid the complexity of electromagnetic actuation, reduce the cost of manual set up and the consequent lack of repeatability and reliability associated with electromagnetic actuators such as torque motors.

Valve actuation using smart materials has been the subject of a number of previous studies. Linder et al. [4] described a servovalve with a spool directly driven by a piezoelectric stack actuator. However, the approach required mechanical amplification in order to obtain sufficient spool displacement. A similar concept is presented in [5], and the authors undertook performance tests at high temperatures. Changbin et al. [6] used a spool that was directly driven by a piezoelectric stack actuator; the major hysteresis loop was measured and phenomenological hysteresis models were discussed, but the final controller did not include hysteresis compensation. A whole family of valves using piezoelectric

elements was developed in RWTH Aachen [7,8]. These papers were focused on the description of the different valve designs using piezoelectric actuation and investigation of their basic performance.

Research into smart materials for hydraulic valves most frequently concern two-stage servovalves. A conventional servovalve has an electromagnetic torque motor providing first-stage actuation, and either a flapper-nozzle, jet pipe or deflector jet as the first hydraulic stage to create a pressure difference across the ends of the main spool. This pressure difference is used to control spool position, which determines the port orifices sizes and hence the main-stage flowrate. The conventional torque motor and first-stage is a complex design including machining processes with tight tolerances, manual assembly, and requiring a very accurate calibration process [9]. In [10] the authors indicate the benefits of utilising piezoelectric actuators compared with torque motors; these include the ability to achieve significant mass reduction, smaller size, a simpler mechanical design and zero power requirement for constant spool position. An increase of torque motor performance is also possible by application magnetic fluids in the air gaps [11]. Piezoceramic materials are one example of a smart material to provide actuation and are characterised by a high dynamic response but small maximum strains, in the region of 0.15%. Therefore, a challenge is to create sufficient displacement for first stage actuation since typically there is a need for a displacement in the region of ±0.1mm. One of the drawbacks of utilising piezoelectric actuation includes the need for complex amplifier electronics and operation at a higher voltage compared to a torque motor. In addition piezoelectric materials suffer from hysteresis, creep and a temperature dependence [12,13], primarily as a consequence of domain motion in the ferroelectric materials employed. A number of piezoelectric actuator designs for valve applications are based on bender actuators [14–16]. Sedziak et al. [14] investigated a servovalve with barometric feedback where the ferroelectric hysteresis of the piezoelectric had a significant influence on the valve flow characteristics. In [17] the authors presented a servovalve where a piezoelectric stack actuator moved a flapper assembly and the displacement of the piezoelectric stack was mechanically amplified. The influence of ferroelectric hysteresis can also be observed in the response of the flow rate versus input voltage. These valves are distinguished by control based on spool or actuator position feedback provided by electrical position transducers. Conversely, [18] presents an aerospace servovalve where a mechanical feedback wire is retained between the spool and piezoelectric bender, which is currently an industry requirement for safety-critical flight controls.

Many smart actuator materials exhibit hysteresis, which prevents accurate and precise open loop control and hinders tuning of closed loop controllers. To better describe this phenomenon, mathematical models of hysteresis have been developed [19], which relate the input and output of the system; rather than being physics-based. An early model was developed by Preisach to describe magnetization effects in ferromagnetic materials [20]. Krasnosel'skii and Pokrovskii proposed a modification of this model [21]. These models use a sum of discrete elements called *operators* or *hysterons*, therefore the quality of the model depends on the number of elements used. In this field a group of Prandtl-Ishlinskii models (classical, modified and generalized) which combines a simple structure and analytical invertability have been developed; the approach provides an easy application for real time hysteresis compensation. The application of a hysteresis model in a piezoelectric servovalve control system has been reported [22], in which a precise fuzzy control algorithm with Preisach hysteresis model in a feedforward loop was proposed to provide better valve performance than PID (proportional integral derivative) control. Nevertheless, the results presented in [22] do not show the accuracy of Preisach model in following hysteresis behaviour. The authors used this model as a feedforward compensator, but it is also possible to perform direct compensation by using the inverse Preisach model. Unlike the Prandtl-Ishlinskii analytical inversion, inversion of the Preisach model is more complicated and its requires numerical operations [23,24]. Furthermore, the presented results are only limited to tracing results of a low frequency (5 Hz) sine wave and do not investigate the performance of this control approach for a dynamic response or at a wider frequency bandwidth. When using smart materials for actuating positioning systems in other applications described in literature [25,26], controllers with hysteresis compensation have shown to provide better performance.

Conventional servovalves also exhibit hysteresis because of magnetization effects in the armature and parts of the core. The technical literature defines hysteresis in flow control servovalves as the difference in the electric current applied to the torque motor coils to generate the same output flow in a test cycle from a negative to a positive rated current. The hysteresis value is presented as a percentage of rated current, and is typically less than 3% [27]. However, in smart actuator materials the hysteresis can be much larger, and presents a very significant obstacle to accurate control. Despite many examples of piezoelectric and other smart material valves being proposed, hysteresis compensation has been rarely investigated to date. Thus the main contribution of this paper is to undertake a detailed investigation of different control strategies to improve the performance of a novel piezoelectric-actuated spool valve using a ring bender, in particular the compensation of hysteresis. The use of a piezoelectric ring bender is particularly attractive since it is well matched to this application in terms of the balance between displacement and force output. The existence of ferroelectric hysteresis is the most common reason that prototype piezoelectric hydraulic valves have not been successful to date. Thus the application of an inverse hysteresis modelling method to this problem, and a detailed comparison of several candidate control schemes incorporating this inverse approach represents a significant contribution to the field.

2. Piezoelectric valve design

The valve concept considered in this work is a small spool valve that is directly controlled by a piezoelectric ring bender. A ring bender is an annular disk that deforms to form a dome in a concave or convex fashion depending on the polarity of the applied voltage. An example of the doming effect of the actuator can be seen in Fig. 1a. Such an actuator configuration has been chosen since a ring bender actuator exhibits a greater displacement than a stack actuator of the same mass, and an increase in stiffness in comparison to similar size rectangular bender [28].

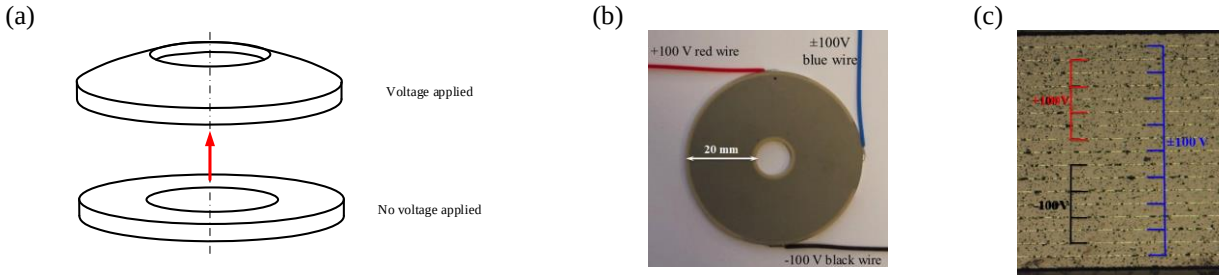

Fig. 1 Piezoelecric ring bender deformation after application of electric field (a), multilayer piezoelectric ring bender (b) electrical connection and (c) cross section of Noliac CMBR08 actuator, the electrode spacing is 67µm for scale.

In this paper a multilayer piezoelectric ring bender, manufactured by Noliac (CMBR08), is used to control the spool. Fig. 1(b) shows the ring bender with its three wire electrical connection. The ring benders are made up of multiple 67 µm thick lead zirconium titanate (PZT) piezoceramic layers. To apply the necessary electric field across the piezoceramic and actuate the device, silver palladium electrodes are located between each layer; see the light regions in Fig. 1 (c). In order to deflect the ring bender in both directions the electrodes are combined into three groups, see Fig. 1 (c). One set of electrodes are maintained at a negative voltage (-100V, black wire), one set are maintained at a positive voltage (+100V, red wire), and the voltage is varied on the intervening electrodes (control electrodes, blue wire) between -100V to +100V. Based on an electrode thickness of 67 µm, the magnitude of the maximum electric field is ~3kV/mm (200V across 67 µm). This electrode configuration allows deflection of the device in both directions since half of the piezoceramic layers expand in-plane, while the other half contract as the control voltage varies from zero to -100V or 100V. When the control voltage is zero the upper and lower half layers experience the same electric field, resulting in no displacement.

A prototype of the piezoelectric actuated spool valve was designed, manufactured, assembled and tested. A cross section of the valve can be seen in Fig. 2 (a) and the complete valve with the piezoelectric actuator is shown in Fig. 2 (b). The ring bender, which is submerged in hydraulic fluid, is attached to hub linked to the spool and to a linear variable differential transformer (LVDT) position sensor. A hydraulic actuator is connected to the valve, however this will not be analysed in this paper. The prototype valve and actuator body was manufactured by additive manufacturing using a laser powder bed fusion process, achieving a significant mass and volume reduction.

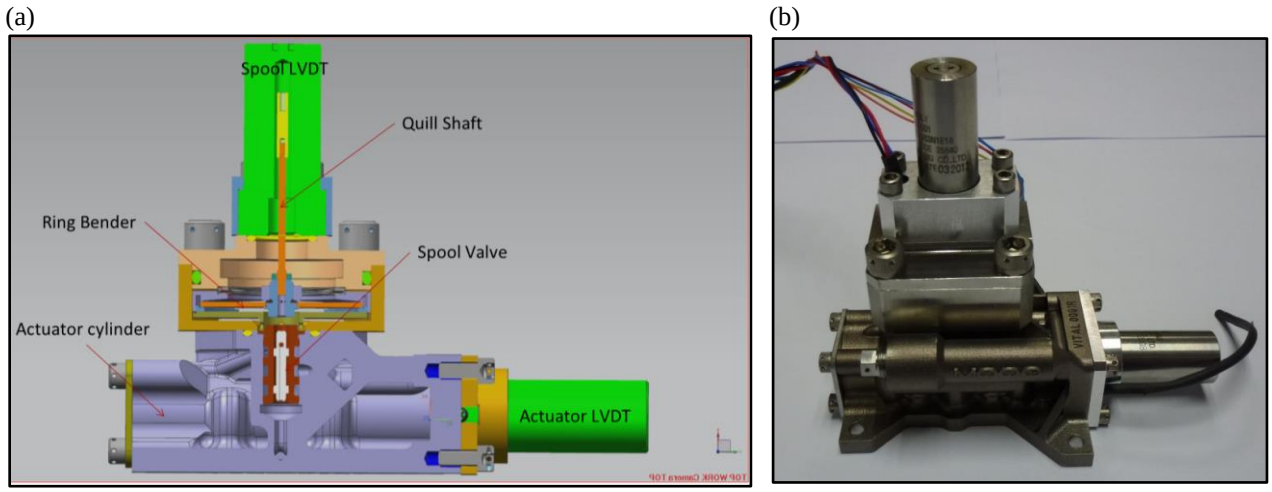

Fig. 2 Piezo valve: (a) cross section of valve, (b) assembled valve with actuator

3. Modelling

3.1. Generalized Prandtl-Ishlinskii hysteresis model (GPIM)

The main characteristic addressed in this paper is the hysteresis exhibited in the piezoelectric actuator, which is universal for such actuators driven by conventional voltage amplifiers [13]. The classical Prandtl-Ishlinskii model is a superposition of weighted play operators and is presented in Fig. 3. Fig. 3(a) represents a classical operator while Fig. 3 (b) is a generalized operator [29]. Due to the symmetrical shape of the single play operator this model can only represent symmetrical hysteresis. Asymmetrical and saturated hysteresis characteristics require modifications of the model structure. Although the hysteretic characteristics of a ring bender may be expected to be symmetrical, in combination with friction and damping occurring in the servovalve, it is in fact asymmetric and reasons will be discussed later. For such situations two popular derivative models have been developed. The first one is a modified Prandtl-Ishlinskii model where weighted superposition of play operators is placed in cascade with a scalar, memory free function represented by a weighted side dead zone operators [30]. This model has been successfully used for modelling saturated hysteresis in magnetic shape memory alloys [31,32]. The second method is a generalized Prandtl-Ishlinskii model, using the generalized play operator [29], and this idea has been developed by Al Janaideh [33–35]. This model is able to reflect complex hysteresis shapes, as demonstrated for shape memory alloys [36,37] and magnetostrictive materials [34]. The advantage of this family of Prandtl-Ishlinskii models is their analytical inversion which enables fast implementation in real time hysteresis compensation systems. In addition these models are more simple to implement than Preisach and Krasnosel'skii-Pokrovskii models [33], as significantly fewer operators are used which accelerates computation time.

Unlike operators from other models (so-called hysterons), the Prandtl-Ishlinskii play operator output value is unlimited. This play operator, denoted by F_r, is the same as 'backlash' which is well known in engineering where it represents clearances between gears. The basic principle is presented in Fig. 3 (c).

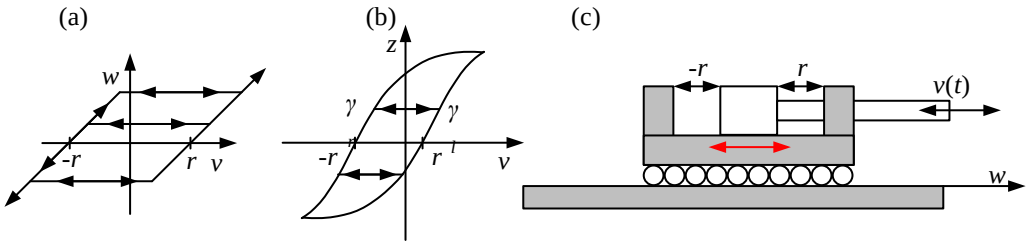

Fig. 3 Classical play operator (a), generalized play operator (b) for Prandtl-Ishlinskii models and (c) mechanical representation of (a) [33,38]

For the input function $v(t)$ which belongs to space $Q[t_0, t_S]$, where space Q represents only a piecewise continuous monotone functions in each time interval $[t_i, t_{i+1}]$, this input function $v(t)$ must fulfil the condition of monotonicity. According to these assumptions the analytical description from $t_0 = 0 < t_1 \ldots < t_N = t_S$, is as follows under conditions that $t_i<t<t_{i+1}$ and $0<i<i_{N-1}$ [33]

$$F_r[v](t) = \begin{cases} \max(v(t)-r, w[v](t_i)) & for \quad v(t) > v(t_i) \\ \min(v(t)+r, w[v](t_i)) & for \quad v(t) < v(t_i) \\ w[v](t_i), & for \quad v(t) = v(t_i) \end{cases} \tag{1}$$

For a full description of a hysteresis model output Y_p, each operator has to be weighted by a density function $p(r)$, which is always positive. The final structure of the model is expressed as (2). A finite number of operators, n, is sufficient to model the hysteresis because the density function tends to zero as the operator number, j, increases. The complete model contains a positive constant ω. The density function $p(r_j) = \rho e^{-\tau r_j}$ is described by three parameters ρ, τ, and α. Where ρ and α are always positive and $r_j=\alpha j$ [33].

$$Y_P(t) = \omega[v](t) + \int_0^r p(r) \cdot F_r[v](t) dr \tag{2}$$

The generalized operator G_r is described by two user defined envelope functions. For an increasing input $v(t)$, the output z of a generalized play operator is expressed by values along the curve γ_l, for a decreasing input, z is expressed by values along the curve γ_r (Fig. 3 (b))[33].

$$G_r[v](t)=\begin{cases}\max(\gamma_l(t)-r, z[v](t_i)) & for \quad v(t)>v(t_i)\\ \min(\gamma_r(t)+r, z[v](t_i)) & for \quad v(t)<v(t_i)\\ z[v](t_i) & for \quad v(t)=v(t_i)\end{cases} \tag{3}$$

The shape of the hysteresis determines the appropriate function to use. For example, hyperbolic tangents can be appropriate to describe saturated hysteresis in magnetic shape memory alloys [37]. In the case of piezoelectric materials simple linear functions $\gamma_l(t)=a_0v(t)+a_1$ and $\gamma_l(t)=b_0v(t)+b_1$, are appropriate to describe the hysteresis shape effectively [33]. A future simplification of the model to envelope functions expressed as $\gamma_l = \gamma_r$ *where* $\gamma_l = a_0x + a_1$ can also provide sufficient modeling and compensation results [34] hence, this approach will be used in this paper. In a similar approach to the classical Prandtl-Ishlinskii model, the generalized $Y_{p\gamma}$ is given by a finite sum of weighted generalized play operators (4), where ω_G is positive constant but in this work it is assumed that $\omega_G = 0$ since hysteresis modelling without this function has also provided satisfying results without increasing model error.

$$Y_{p\gamma}(t)=\omega_G[v](t)+\sum_{j=0}^{n}p(r_j)\cdot G_{r_j}^{\gamma}[v](t)dr \tag{4}$$

3.2. Inverse generalized Prandtl-Ishlinskii model

The application of an inverse model H^{-1} to compensate hysteresis is schematically presented in Fig. 4, which shows that the input $y_h(t)$ is initially input into the inverse model where it is transformed to a value $u(t)$. The output of the inverse model is then applied as an argument to object with the hysteresis H, as a modified voltage (in the case of piezoelectric materials). Based on an inverse function theorem, perfect compensation leads to the input and output signals being equal, $y_h(t) = y(t)$. The inverse generalized Prandtl-Ishlinskii model is a cascade of inverse envelope functions (5) [34].

$$Y_{P\gamma}^{-1}(t)=\begin{cases}\gamma_l^{-1}\left(\sum_{j=0}^{n}\hat{p}(r_j)F_{\hat{r}_j}[v](t)\right) & for \quad \frac{dv}{dt}\geq 0\\ \gamma_r^{-1}\left(\sum_{j=0}^{n}\hat{p}(r_j)F_{\hat{r}_j}[v](t)\right) & for \quad \frac{dv}{dt}\leq 0\end{cases} \tag{5}$$

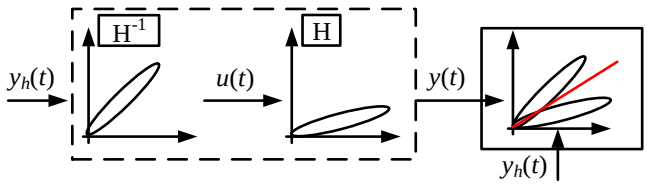

Fig. 4 The approach of cascade hysteresis compensation by an inverse model

The inverse model requires both inverse threshold and density function values. These are obtained from parameters identified from measured data, which is possibly due to an initial loading curve concept, which was proposed and described by [29] as an alternative method for hysteresis description. Based on this concept the inverse model is analytically available, which was investigated in detail and presented in [13,30,34]. Threshold values, which describe the play operator $F_{\hat{r}_j}$ in the inverse model, are given by (6). The density function for the inverse model is given by (7) and (8) [34].

$$\hat{r}_j=\sum_{i=0}^{j}p_i(r_j-r_i) \tag{6}$$

$$\hat{p}(r_0)=\frac{1}{p(r_0)} \quad for \quad i=0 \tag{7}$$

$$\hat{p}(r_j) = \frac{1}{\sum_{i=0}^{j} p(r_j) - \sum_{i=0}^{j-1} p(r_j)} \quad for \quad i \in \langle 1; j \rangle \tag{8}$$

3.3. Valve modelling

A schematic view of the valve can be seen in Fig. 5, where the piezoelectric ring bender (left of image) and the spool is shown. When a control voltage is applied to the piezoelectric ring bender it displaces, as in Fig. 1 and thereby moves the spool. As the spool moves in the positive x direction this will connect the supply pressure (P_s) to the control port 1 (P_1) and return pressure (P_r) to the control port 2 (P_2).

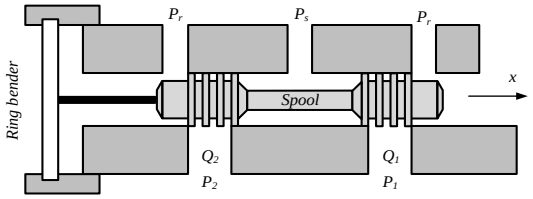

Fig. 5 Piezoelectric valve schematic showing ring bender (left of image) and spool position

The dynamic response of the valve spool motion to the ring bender control signal is determined by:

i. the power amplifier bandwidth, and its current limit which limits the rate of change of output voltage given that the piezoelectric actuator behaves approximately like a capacitor,
ii. the friction, damping and inertia associated with ring bender and spool motion,
iii. flow forces acting on the spool as the ports open.

These dynamic characteristics lead to a complex, non-linear valve response, modelled in detail in [3]. However, in this work an off-line control algorithm based on a low order 'black box' model has been identified as a least-squares fit to input-output measurements. The amplifier input signal was a sine wave sweep of 5V amplitude (form 0 to 10V), and frequency from 0.2 to 250 Hz. At low frequency this amplitude corresponds to 100V amplitude applied to the ring bender and 70μm output position amplitude. The spool position was measured by the LVDT position sensor connected to the spool, see Fig. 2(a). The resulting second order transfer function is expressed by equation (9). The identified transfer function is compared to the valve frequency response in Fig. 6, with steady state magnitude normalized to unity. Note that the additional phase lag at low frequency is a non-linear effect, resulting from the hysteresis. The second order model is sufficient to approximate the characteristics up to 250Hz since the phase lag is no more than -180° in this frequency range. More precise modelling needs to include higher order model and non-linearities, as shown in [3].

$$G_v(s) = \frac{1.2x10^6}{s^2 + 2900s + 1.2x10^6} \tag{9}$$

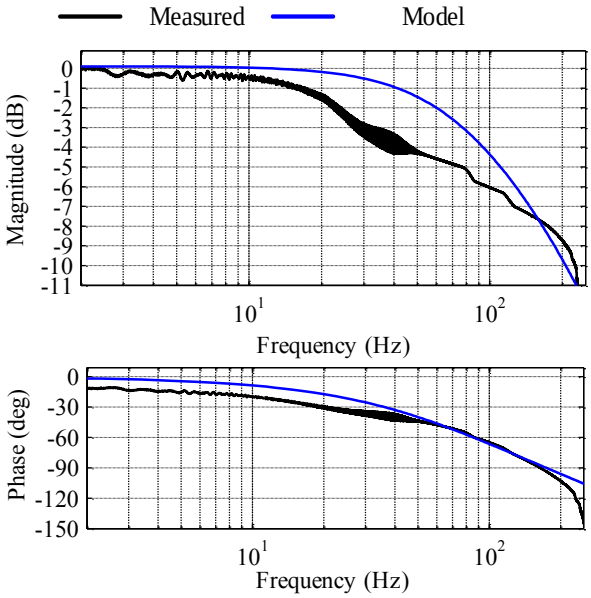

Fig. 6 Measured and model frequency response (magnitude and phase) from the amplifier input to spool position

4. Control

4.1. Alternative control strategies

The valve performance is directly related to the accuracy of spool positioning, and thus hysteresis is a major issue in achieving optimum performance. In a piezoceramic actuator, hysteresis is observed between the applied voltage and charge, and charge is proportional to displacement. In this section control strategies, used to reduce this effect, will be presented; six control strategies will be compared.

Test data for hysteresis modelling were collected during application of a voltage input signal $u(t)$ to the amplifier. The output in this case is the open loop (OL) spool movement $y(t)$, as shown in the Fig. 7 (a), where H is the hysteresis and $G(s)$ is the dynamic behaviour of the valve. After identification of the GPIM parameters, the inverse GPIM (or IGPIM), H^{-1}, was introduced to modify the valve control signal as in Fig. 7 (b). In this case the desired position of the valve $y_0(t)$ is processed by the IGPIM to supply a voltage signal $u(t)$ to the voltage amplifier. The resulting output position of the valve spool, $y(t)$, ideally should exhibit no hysteresis behaviour. This strategy is tested to examine the hysteresis reduction performance of the IGPIM.

The first closed loop strategy employed uses a proportional-integral-derivative (PID) compensator, as in Fig. 7 (c). The desired spool position $y_0(t)$ is compared with the actual position $y(t)$. The resulting control error, $e(t)$, is processed by the PID compensator to provide a voltage signal $u(t)$. The second closed loop scenario consists of the PID compensator in series with the IGPIM (Fig. 7 (d)). The idea of this strategy is to use the inverse model to reduce the nonlinear behaviour of the valve and simplify the control problem to control of a linear system. The next strategy uses the inverse GPIM as a feedforward hysteresis compensator to reduce the influence of the hysteresis behaviour on the system. A PID controller in parallel is used to reduce the remaining control error. The inverse model output voltage signal, $u_1(t)$, and the PID output, $u_2(t)$, are added to give the valve control signal, $u(t)$.

With the feedforward (FF PID) strategy, a sudden change in demand will lead to a control signal much greater than the steady state value required due to large contributions from both $u_1(t)$ and $u_2(t)$ [39]. To reduce this, the valve dynamic model $G_v(s)$ (an estimate of $G(s)$) can be introduced, as in Fig. 7 (f). The predicted position signal $y_1(t)$ should be similar to the measured position $y(t)$. The assumption in this work is that a system response which is the same as $G_v(s)$ is adequate, and the purpose of the closed loop controller is to correct for modelling errors or parameter variations that would cause the response to deviate from this simple model.

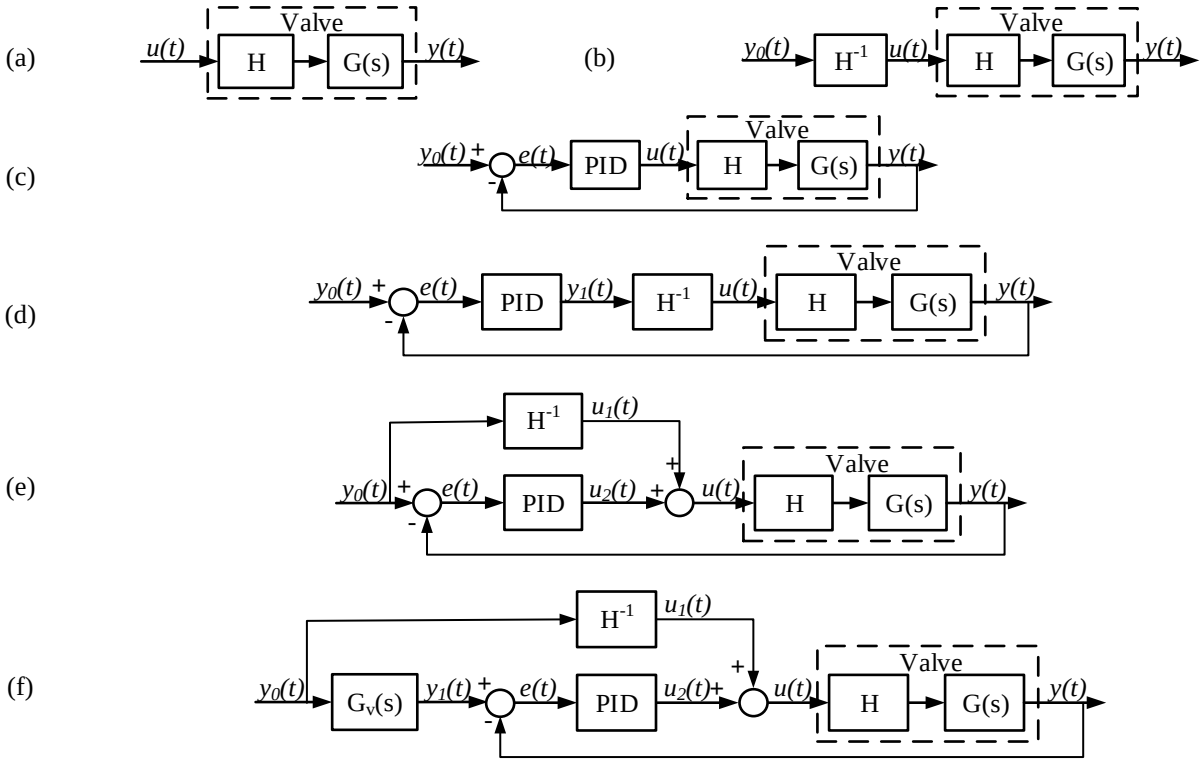

Fig. 7 Control strategies (a) open loop, no hysteresis compensation (OL), (b) open loop hysteresis compensation strategy (OL HC), (c) PID closed loop control strategy (PID), (d) PID closed loop with hysteresis compensation control strategy (PID HC), (e) feedforward hysteresis compensation with PID closed loop control strategy (FF PID), (f) feedforward hysteresis compensation with valve model and PID closed loop control strategy (FF PID G).

4.2. Controller implementation – PID controller description

The PID controller is the most popular closed loop industrial controller which is frequently used for fluid power applications because of its simplicity and easy application in real time control systems [40,41]. The mathematical expression of this controller is given in (10). Three gains K_p, K_i and K_d scale the proportional, integral and derivative part of the controller, respectively. However, finding the optimal values for the gains is not straightforward [42].

$$u(t) = K_p e(t) + K_i \int_0^t e(\tau) d\tau + K_d \frac{de(t)}{dt} \tag{10}$$

where $u(t)$ is the command signal, and $e(t)$ is the system error.

In this paper, PID controller tuning is acheived by using the proprietary MathWorks PID tuning algorithm available in the simulink control design toolbox [43]. A Simulink model for each control scenario was prepared, using the identified dynamic model, $G_v(s)$, GPIM and the inverse hystersis model. The first value of K_p and K_i, presented in the Table 1, was tuned for a response time of 0.01s and with good reference tracking settings. The algorithm linearizes the prepared model and tries to find a balance between the response time and reference tracing settings [43,44]. The other controller gains in Table 1 were manually adjusted on a test stand in an attempt to improve behaviour of the system in terms of settling time and overshoot. In all cases the automatic tuning of gain K_d gave zero. In practice a non-zero K_d leads to oscillatory behaviour of the spool due to unmodelled high-frequency dynamics, and so K_d was set to zero for all control scenarios. The K_p and K_i values are different for the six control methods due to the different ways in which hysteresis is compensated: the plant as controlled by the PID controller is effectively different in each case.

5. Results

5.1. Test rig

A prototype of the piezoelectric ring bender spool valve was assembled and tested on a dedicated test bench (Fig. 8 (a) and (b)). All the tests were performed at 100 bar and the power pack supplies hydraulic fluid at a constant temperature. The piezoelectric ring bender was actuated by a Noliac NDR6220DC voltage amplifier. The amplifier input voltage was set from 0 to 10V, which corresponds to a variable output voltage from -100V to +100V respectively. During all tests the ring bender was submerged in hydraulic oil. The data acquisition and the real time controller platform was an 'xPC system' using a National Instruments (NI) PCI card, connector block, Host PC and a Target PC. This system uses a real-time auto-coded Simulink model to program the control schemes. All the input and output signals were received or sent out through the NI connector. The data analysed were command signal (commanded position of the ring bender), command voltage (signal to the amplifier), amplifier output voltage, and ring bender-spool position. The sampling time for all the tests were 10 kHz.

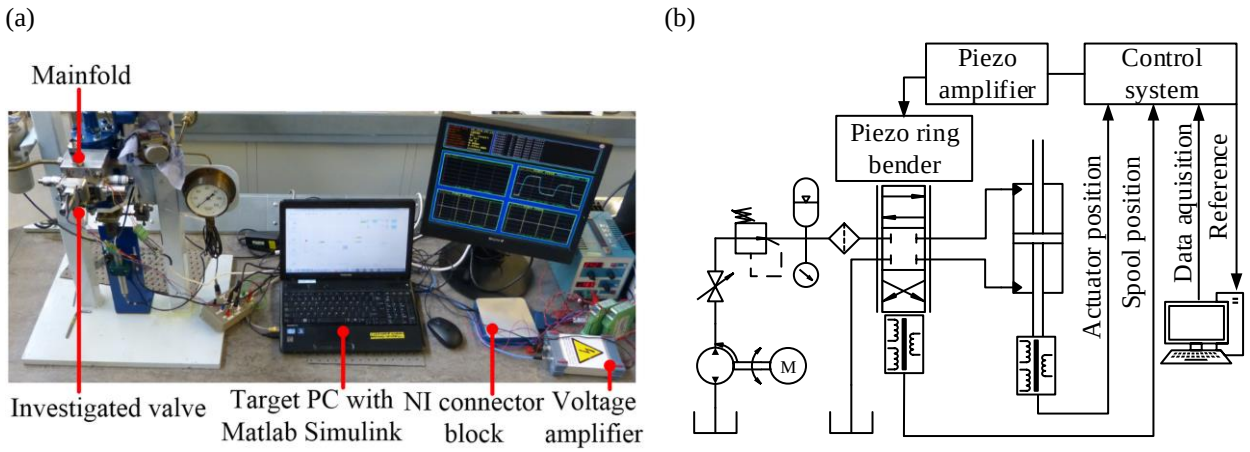

Fig. 8 Test rig (a) configuration, (b) schematic

5.2. Identification of hysteresis model parameters

The parameters of the GPIM must be estimated from real test data. To evaluate the main and minor loops of the hysteresis and the relationship between them, a harmonic damped input signal described by the equation (11) was used. This signal will be also used as a training signal for the hysteresis model parameter estimation. To unify the measurement conditions and avoid the occurrence of arbitrary states of the piezoelectric actuator, as a result of hysteresis, a synchronization procedure was employed. Before each measurement a damped sine signal was applied to the valve and the measurements started when the command signal, valve output and compensator output were at zero value.

$$v_{trening}(t) = \begin{cases} 5 & for\ t \in \langle 0;\ 1.25s \rangle \\ 5 + 5\sin(2\pi \cdot 0.2(t - 1.25)) & for\ t \in \langle 1.5;\ 10s \rangle \\ 5 + 5\sin(2\pi \cdot 0.2(t - 1.25)) \cdot (1 - 0.02(t - 10)) & for\ t \in \langle 10;\ 60s \rangle \end{cases} \quad (11)$$

The spool position is plotted against time in Fig. 9 (a) and against command voltage in Fig. 9 (b). The maximum deflection of the piezoelectric spool assembly is approximately ±70 µm and the maximum hysteresis width is 17.2 % of the full movement range. The hysteresis loops are almost symmetric with a small movement restriction that can be seen at both sides of the loop, caused by mechanical friction. Modelling attempts indicate good accuracy of the hysteresis model when using envelope functions expressed as $\gamma_l = \gamma_r$ *where* $\gamma_l = a_0 x + a_1$ – which was also proposed in [34]. This was found to provide modelling error equal to 3.3 µm peak error and compensation error equal to 3.68 µm peak error. In this case the generalized play operator is symmetric and similar to the classical play operator. The constants a_0 and a_1, which change the operator's slope and offset, have an influence on the model accuracy and continues to lead to a difference compared to the classical PI model. The GPI model could be reduced to the classical PI model, while applying $y_l = y_r$ and $y_l = v$ [34]. As seen in Fig. 9 (a) the GPIM can model the valve sinewave response very well. In addition, Fig. 9 shows that the movement restriction at the loop ends are approximated with sufficient accuracy, the maximum peak modelling error is 3.3 µm (Fig. 9 (c)), which is 2.36% of the full displacement. The parameters of the model are as follows: $a_0 = 0.9647$, $a_1 = 0.1014$, $\alpha = 0.4193$, $\rho = 5.8387$, $\tau = 1.0302$. The number of operators n=15 was chosen as a trade-off between complexity and precision of the model. Values of these parameters were obtained by a nonlinear least squares fit [45].

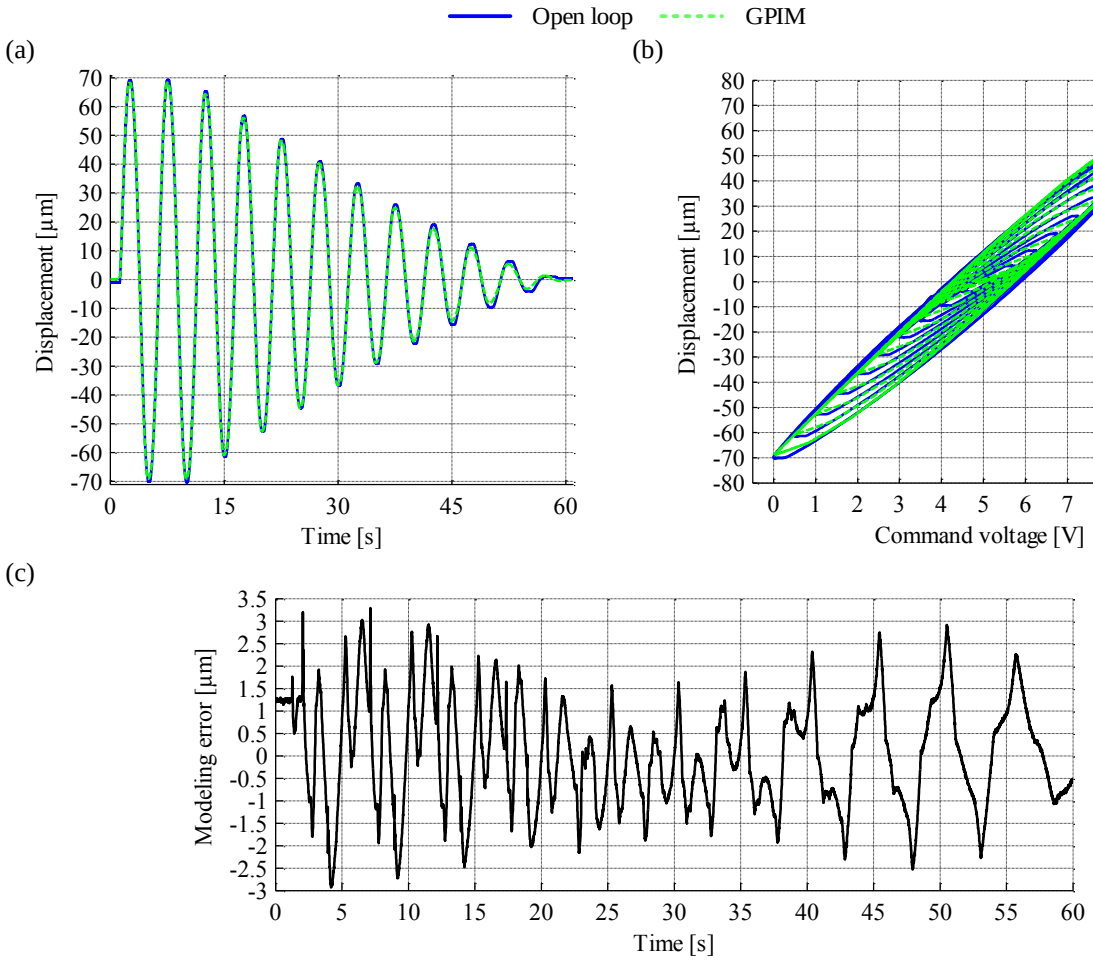

Fig. 9 Valve (blue) and model output (green) (a) for the training signal in time domain, (b) Valve and model output for the training signal in time command voltage domain, (c) GPIM modelling error

5.3. Open loop control with hysteresis compensation

In order to compensate for the nonlinear behaviour of the piezo-spool assembly an inverse GPIM (IGPIM) was prepared based on the estimated parameters and expressions described in section 3.2. In this test the inverse model was used as a series compensator, as shown in Fig. 7 (b). The open loop control with hysteresis compensation achieved a hysteresis reduction of an average of 2.03 µm (1.45% of the full movement range), which is clearly visible in Fig. 10 (a) and Fig. 10 (b). The maximum error, presented in Fig. 11, was connected with a modelling inaccuracy at the loop turns and is equal to 3.68 µm, which is 2.63 % of the movement range. The output of the IGPIM, presented in Fig. 12, is a voltage reference which was applied to the amplifier to achieve the hysteresis compensation.

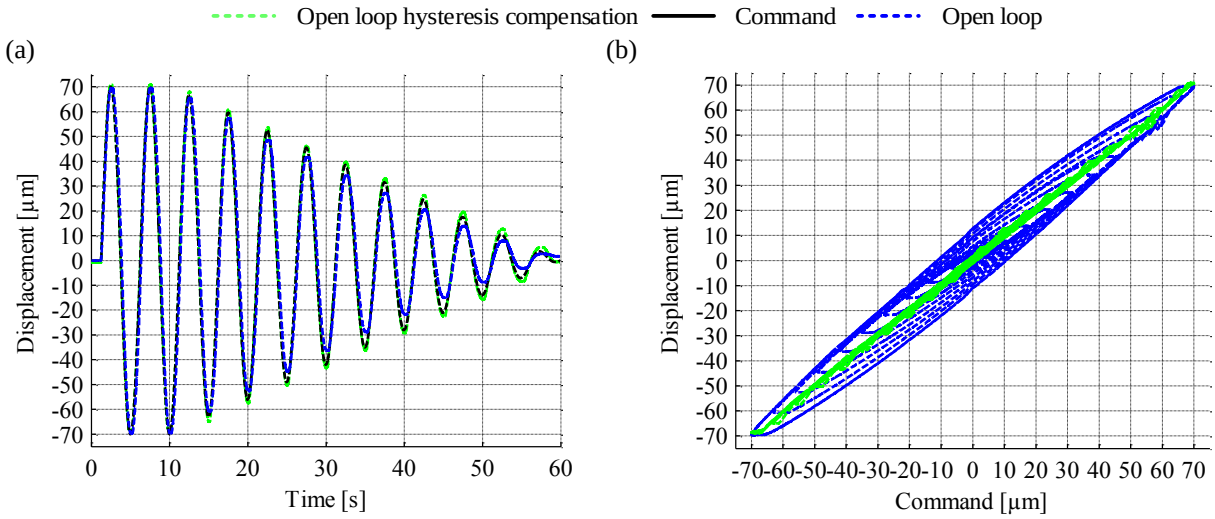

Fig. 10 Training signal (a) valve's output, (b) valves hysteresis and compensation result.

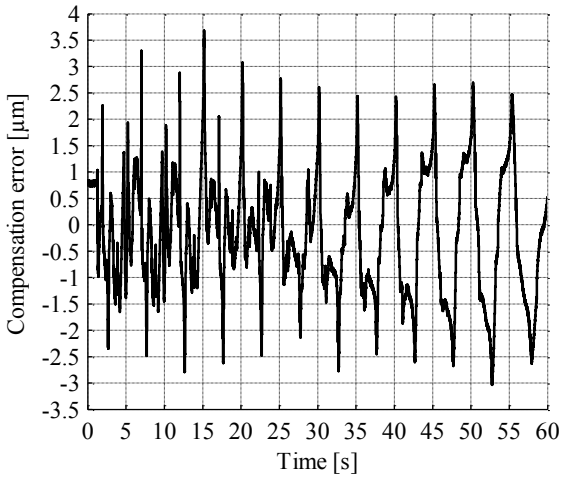

Fig. 11 Hysteresis compensation error

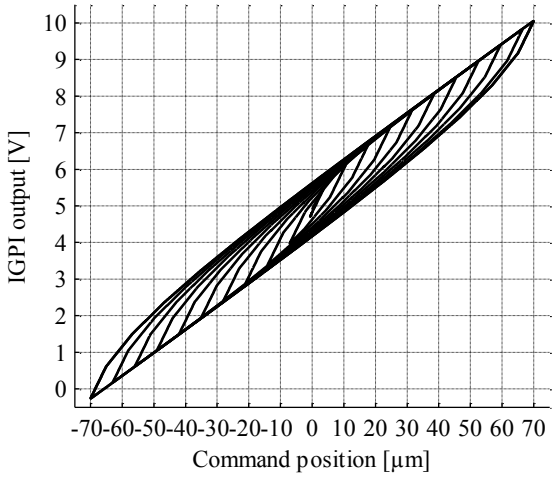

Fig. 12 Output of the IGPIM

For validation purposes another more complex input signal was applied to the inverse model with the aforementioned parameters. The validation signal was a combination of trigonometric functions as in (12). The response for this signal is shown in Fig. 13 against time and against command voltage in (cases (a) and (b)). Fig. 13 (c) shows that the modelling error has increased up to 4.22 µm, which is 3.02% of the full movement range.

$$F(t) = \sin(2\pi \cdot t \cdot 0.35) + 2\cos(2\pi \cdot t \cdot 0.2 + \pi/2) + 2\sin(2\pi \cdot t \cdot 0.3 + \pi/2)$$

$$v_{\text{verification}}(t) = F(t+8), \ \textit{for } t \in \langle 0; 53s \rangle \tag{12}$$

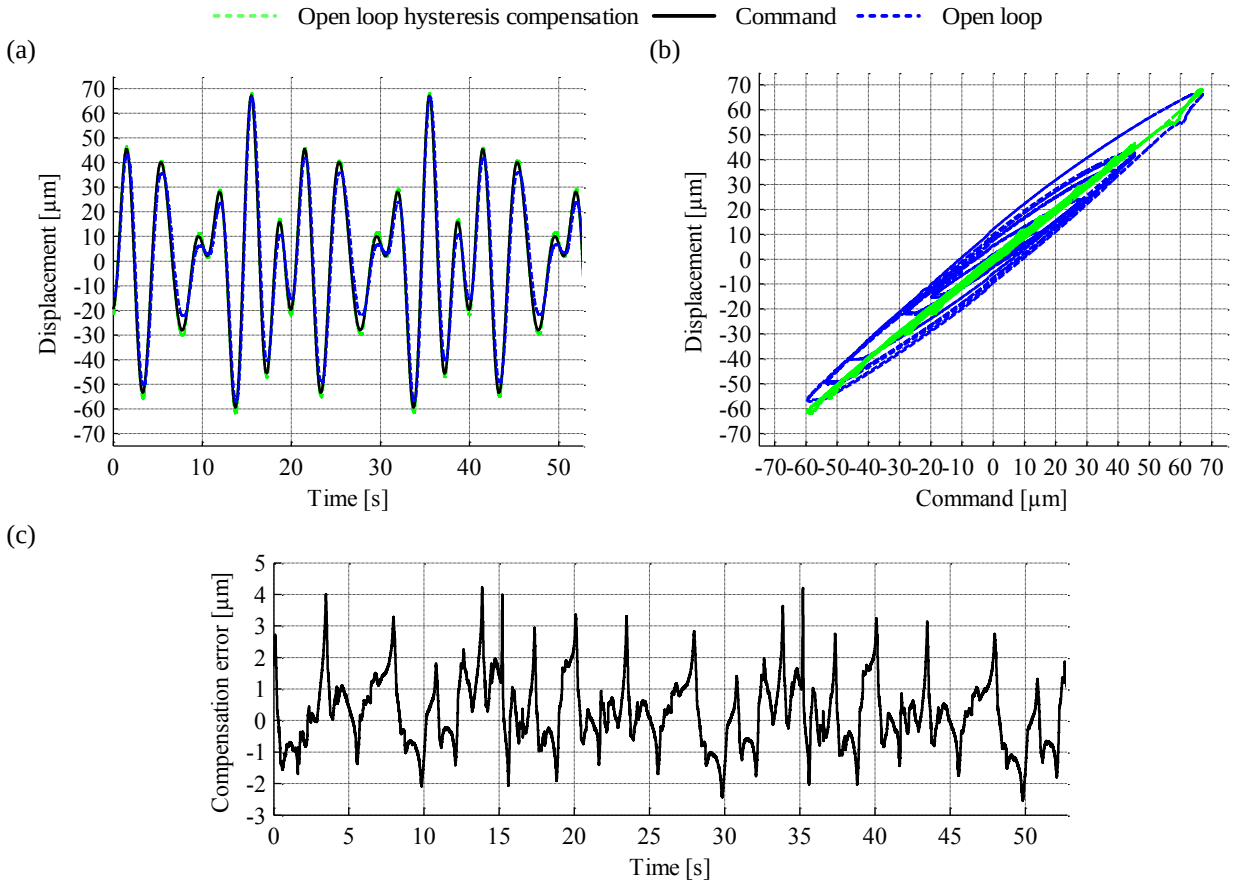

Fig. 13 Verification signal (a) valve output, (b) valves hysteresis and compensation result, (c) hysteresis compensation error

5.4. Closed loop control experimental results

The control performance is shown in two ways: (i) step responses for different reference step sizes and (ii) frequency response for different displacement amplitudes. For each case study all the control strategies were tested. The results are compared by the settling time and overshoot for step responses and -3 dB amplitude frequency and -90 degree phase shift frequency for the frequency responses.

5.4.1. Step response results

Three step response amplitudes were chosen to show different valve working points. The step sizes were up to ±70 µm, where 0 µm is the neutral position with all ports closed as in Fig. 5. The spool overlap is approximately ±25 µm from the neutral spool position. The first step was from 0 to 17.5 µm (reference amplitude 17.5 µm), the second from -17.5 to 35 µm (reference amplitude 52.5 µm) and the third from -52.5 to 35 µm (reference amplitude 87.5 µm). These steps correspond to spool movement in the overlap area, spool movement from a closed valve to positive open valve position and spool movement from a negative open valve to positive open valve position respectively. The settling time criterion is fulfilled when the spool position reaches and stays within ±5% of the current step amplitude. The overshoot is calculated as the ratio of the peak spool position and the current step amplitude. The results for step responses for all closed loop control strategies are presented in Table 1. For this study a ramp command over 2 ms was used rather than a pure step, since an ideal step command reached the device's current limit (1.5 A peak current).

Table 1
Results for different control scenarios and PID constants

Controller	Acronym	K_p	K_i	Settling time 5% (milliseconds)				Overshoot (%)			
Reference amplitude (µm) →				17.5	52.5	87.5	Avg.	17.5	52.5	87.5	Avg.
PID closed loop control	PID 1	1.1987	474.5090	11	4.8	5.7	7.2	7.99	4.06	0.41	4.2
	PID 2	2.3968	949.0180	10.3	11.8	8.1	10.1	33.87	0.68	0.30	11.6
	PID 3	0.5992	474.5090	16.7	13.9	12.7	14.4	15.86	16.24	14.88	15.7
	PID 4	1.1987	949.0180	22	9	9.2	13.4	42.61	19.62	10.37	24.2
	PID 5	1.1987	237.2552	22.7	21.6	19.4	21.2	2.40	0.97	0.55	1.3
	PID 6	0.5992	237.2552	14.3	15.2	14.1	14.5	2.58	1.21	0.58	1.5
PID with hysteresis compensation	PID HC 1	0.4823	190.9162	14.2	17.0	17.1	16.1	2.05	0.97	0.58	1.2
	PID HC 2	0.4823	213.8982	11.4	15.1	14.5	13.7	2.75	1.09	0.69	1.5
	PID HC 3	0.9645	427.7964	12.2	9.8	6.5	9.5	4.67	1.27	0.72	2.2
	PID HC 4	1.4468	641.6946	10.6	7.6	7.2	8.5	6.94	1.09	0.69	2.9
	PID HC 5	1.6879	748.6437	4.1	7.2	7.4	6.2	1.92	3.44	3.67	3.0
	PID HC 6	1.4468	748.6437	4.4	11.7	7.4	7.8	7.17	5.59	4.34	5.7
Feedforward hysteresis compensation with PID	FF PID 1	1.1987	474.5090	11.7	15.5	18.3	15.2	52.57	36.58	25.90	38.4
	FF PID 2	0.5992	474.5090	21.9	20.3	18.9	20.4	58.69	39.73	27.33	41.9
	FF PID 3	1.1987	949.0180	19.2	17.4	18.1	18.2	75.82	39.32	27.09	47.4
	FF PID 4	1.1987	237.2552	20.1	23.0	23.1	22.1	39.11	29.76	21.81	30.2
	FF PID 5	0.5992	237.2552	20.2	20.1	21.9	20.7	37.36	34.07	25.09	32.2
	FF PID 6	0.2996	118.6276	34.7	29.9	29.7	31.4	20.23	26.09	21.84	22.7
Feedforward hysteresis compensation with valve model and PID	FF PID G 1	1.1987	474.5090	11.9	10.7	5.7	9.4	13.11	10.72	3.18	9.0
	FF PID G 2	2.3968	949.0180	13.3	4.9	5.9	8.0	8.74	2.74	1.75	4.4
	FF PID G 3	0.5992	474.5090	13.5	5.2	5.6	8.1	8.92	4.72	2.31	5.3
	FF PID G 4	1.1987	949.0180	13.7	4.8	5.7	8.1	8.92	2.04	3.08	4.7
	FF PID G 5	0.5992	237.2552	34.1	16.6	6.7	19.1	12.59	7.11	4.61	8.1
	FFPID G 6	0.2996	118.6276	5.2	10.8	11.7	9.2	5.77	6.35	7.59	6.6

The open loop (OL) and open loop with hysteresis compensation (OL HC) step responses are shown in Fig. 14, where three different step sizes are presented in (a) 17.5 µm, (b) 52.5 µm, (c) 87.5 µm. As can be seen the OL response has different start values and the commanded value cannot be achieved because of the hysteresis behaviour of the piezoelectric ring bender. The OL HC response has a constant start value error due to inaccuracy of the inverse model. The commanded value is reached for all values, but is not maintained due to creep of the piezoelectric. Creep is a gradual change of ring bender deformation with time while the command voltage is constant, and this is due to slow ferroelectric domain motion in the piezoelectric material. However, the piezo-spool assembly response time (10 milliseconds) is good even without control.

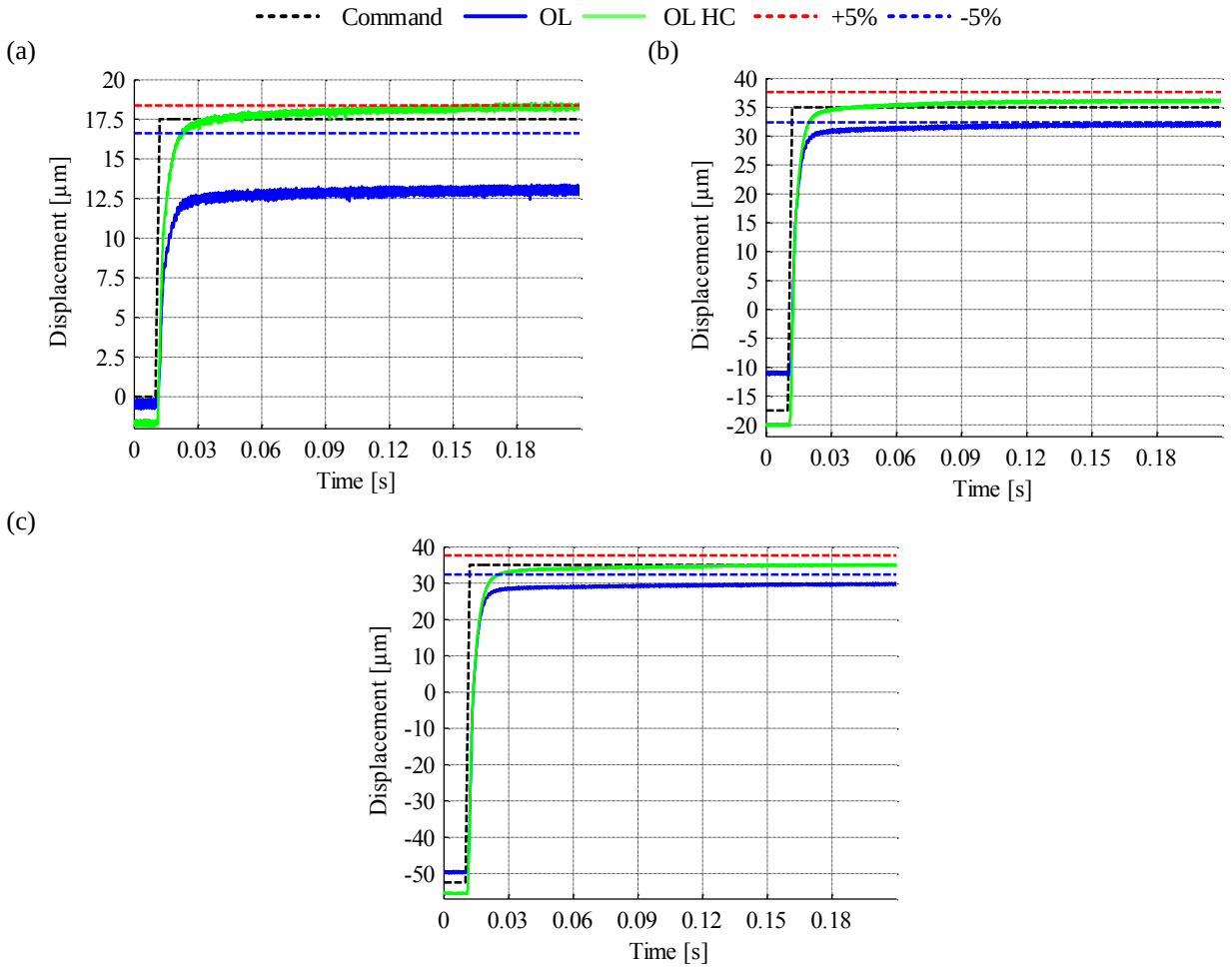

Fig. 14 OL and OL HC step response for step sizes (a) 17.5 µm, (b) 52.5 µm, (c) 87.5 µm

The step response results for the closed loop PID controller are presented in Fig. 15 (a), (b), (c). The PID 1 variant has the fastest settling time for all step amplitudes. Furthermore, the overshoot does not exceed 8% which makes this PID variant the best of those examined. Compared to other variants the PID 1 is a good compromise between lower overshoot (PID 5 or PID 6) and lower settling time (PID 2).

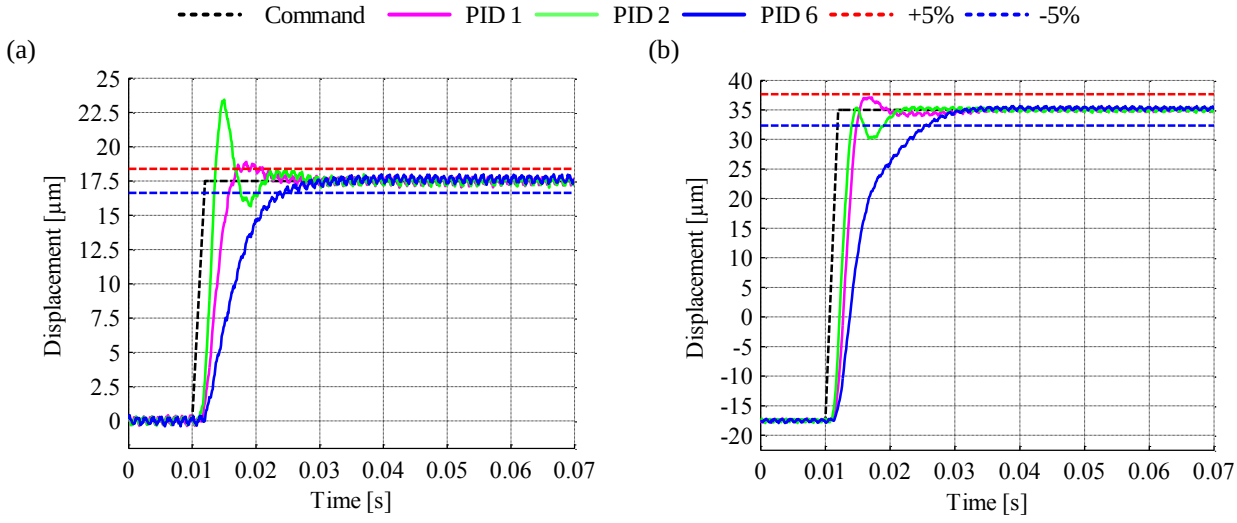

(c)

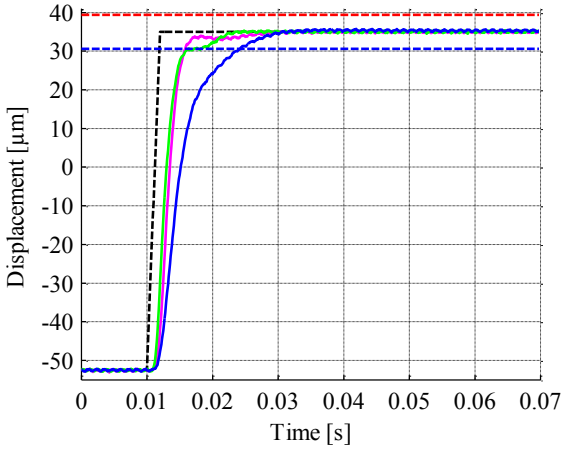

Fig. 15 The PID step response for step sizes (a) 17.5 µm, (b) 52.5 µm, (c) 87.5 µm

The step response results for the closed loop PID with hysteresis compensation (HC) control scenario are presented in Fig. 16 (a), (b), (c). The best variant is in this case PID HC 5, with an average settling time for all amplitudes, equal to 6.2 ms, which is 1 ms faster than for PID 1 and average overshoot reduced by 1 % from 4.15% for PID to 3.01% for PID HC. The applied gains for PID HC are in a similar range to those used for PID without hysteresis compensation. Nevertheless a significant reduction of overshoot (46.5%, comparing the average overshoot of PID 1 and PID HC 3) can be seen comparing these two strategies. This is because the control error *e(t)* is reduced by cancelling the valves hysteresis.

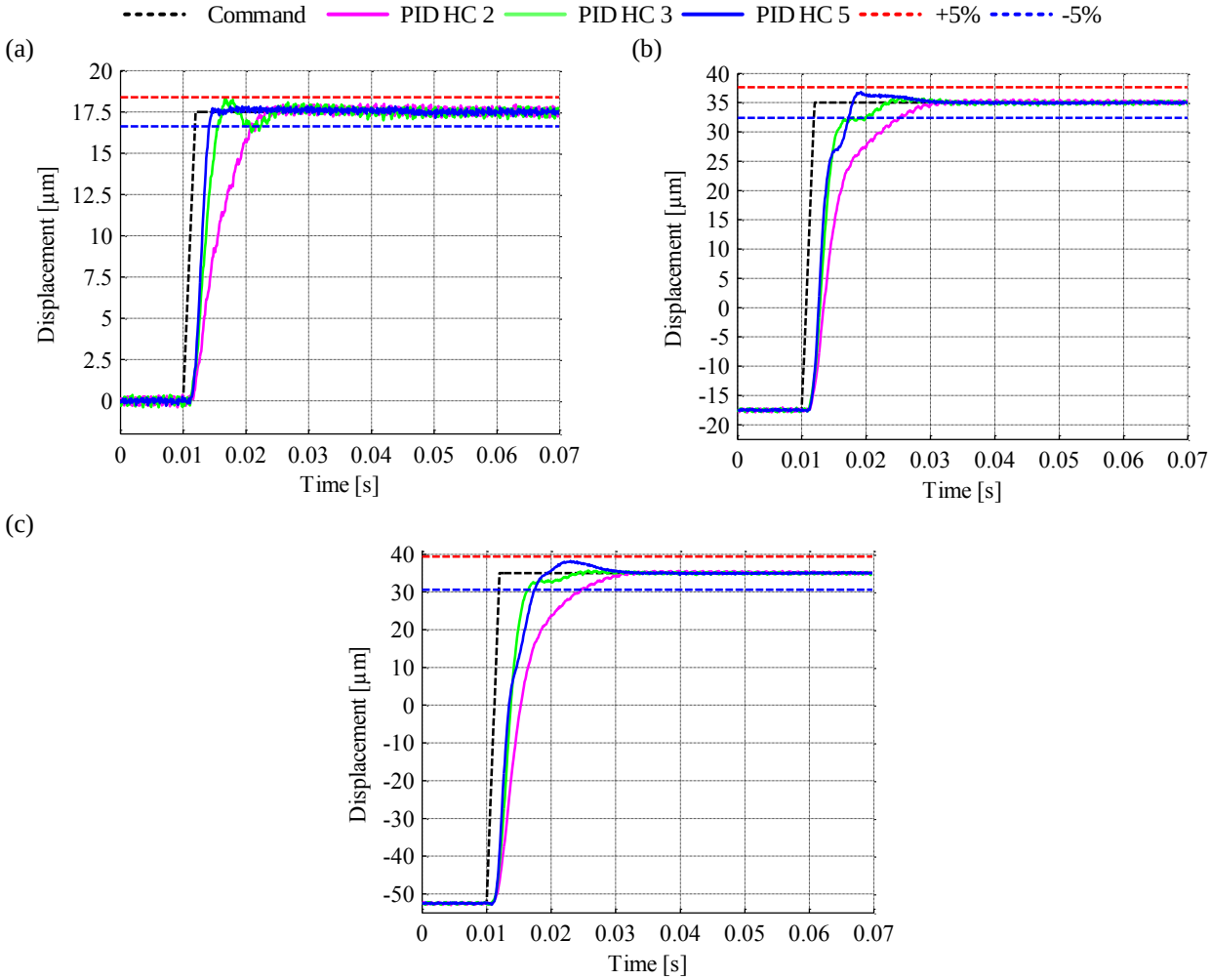

Fig. 16 PID HC step response for (a) 17.5 µm, (b) 52.5 µm, (c) 87.5 µm

The step response results for closed loop feedforward hysteresis compensation with PID control (FF PID) are presented in and Fig. 17 (a), (b), (c). The overshoot and settling time values are much larger than other control scenarios, for example on comparing the average overshoot and settling time values of FF PID 1 and PID 1 the control scenarios were increased by a factor of over 2 and over 9 times respectively. The origin of this problem is that the PID and IGPIM are both trying to cancel the hysteresis and the sum of these efforts leads to the overshoot.

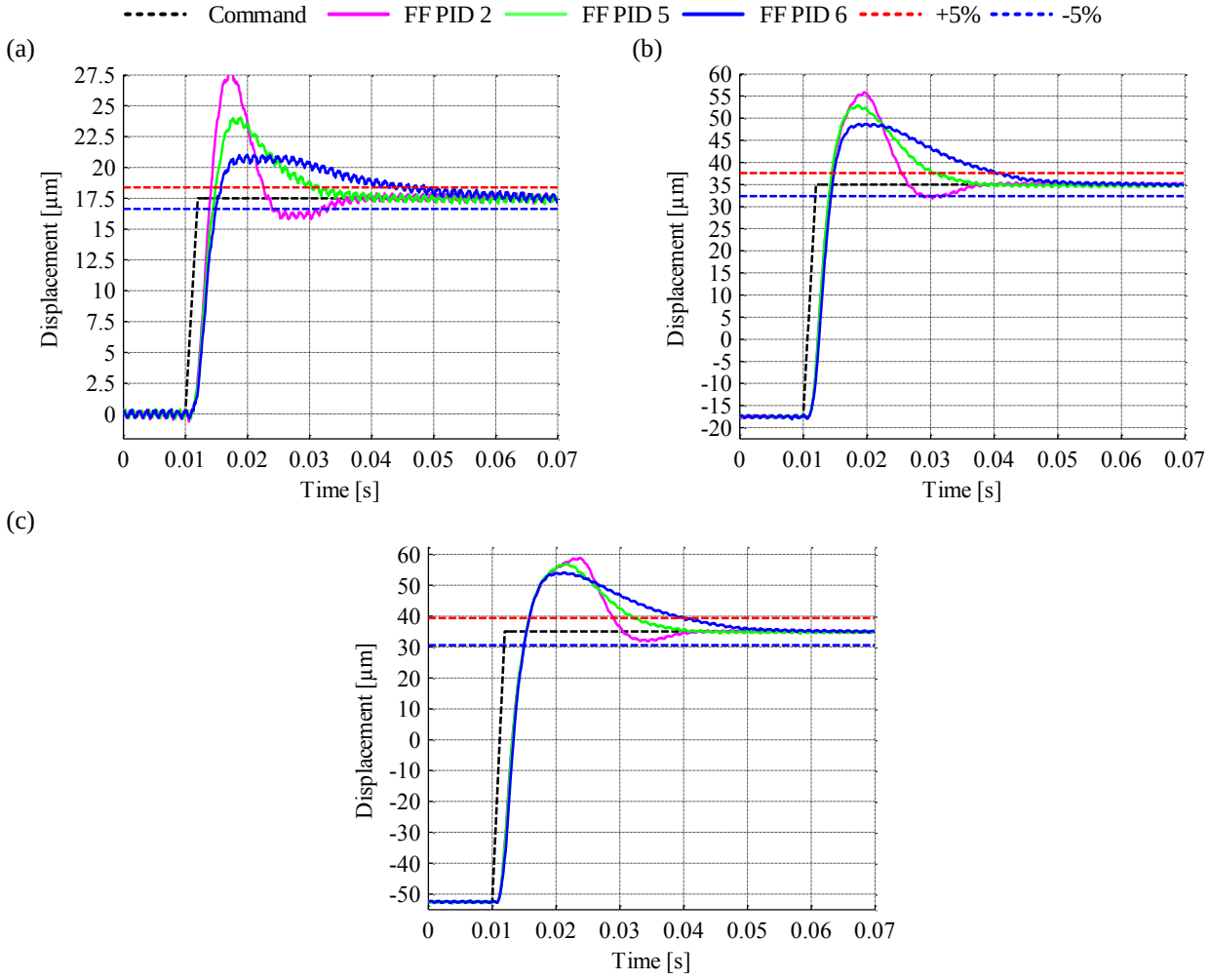

Fig. 17 The FF PID step response for (a) 17.5 µm, (b) 52.5 µm, (c) 87.5 µm

The step response results for closed loop feedforward hysteresis compensation with valve model and PID control (FF PID G) are presented in and Fig. 18 (a), (b), (c). The overshoot problem was resolved by introducing the simplified dynamic model $G_v(s)$ before the control error calculation. As a result, the response overshoot was reduced and is lower than for the PID scenario with the same gains. The best set of gains is FF PID G 6 with an overshoot of 7.6% and settling time of 10.8 milliseconds. Compared to the PID 1, the average settling time is similar but the PIF FF G overshoot is larger by about 2.4%. Compared to the PID HC, the FF PID G controller gives inferior overall performance for step responses.

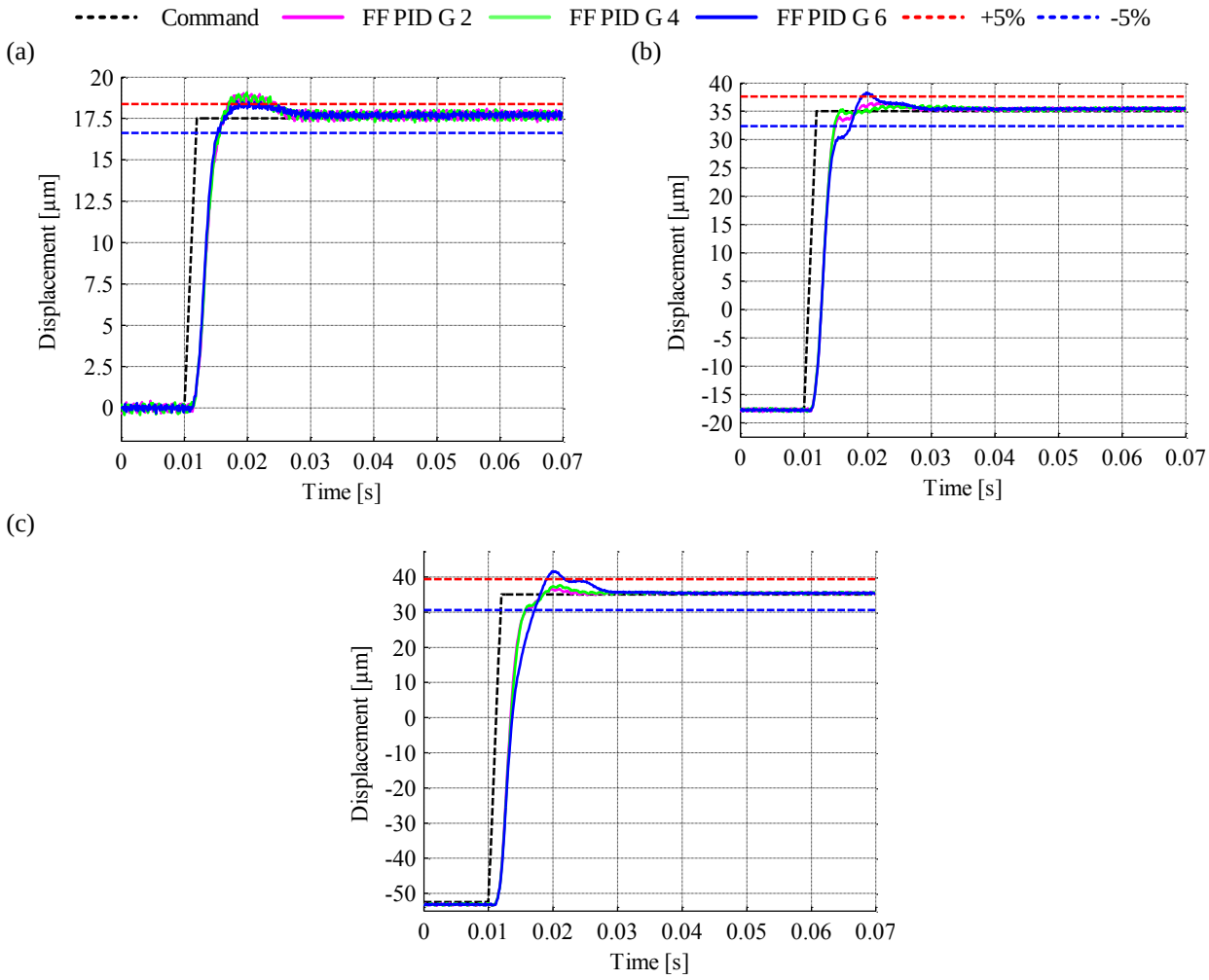

Fig. 18 FF PID G step response for (a) 17.5 µm, (b) 52.5 µm, (c) 87.5 µm

5.4.1. Frequency response results

The two amplitudes used for frequency response testing were chosen to demonstrate the valve's behaviour for 50% (35 µm) and 70% (49 µm) of spool displacement. Both amplitudes correspond to the valve operating from a negative to positive flow, but in different flow ranges. For these tests, the bandwidth (in terms of -3 dB frequency, and -90° frequency) and amplitude overshoot above 0 dB (resonant peak) are presented in Table 2. Only three of the sets of gains presented in Table 2 were tested for each controller, selected on the basis of the lowest settling time. The feedforward PID FF controller was not evaluated here because of the large settling time and overshoot compared to the other control strategies. Frequency responses are estimated from swept sine tests up to 250Hz.

Table 2
Frequency response results

Controller:	Reference amplitude (µm)	OL	OL HC	PID			PID HC			FF PID G		
				1	2	3	4	5	6	2	4	6
-3 dB	35	25.1	39.6	96.1	164.6	77.6	119.5	124.9	118.7	102.5	102	109.9
frequency (Hz)	49	26.7	34.9	76.6	88.4	68.8	79.8	76.8	76.8	86.4	87.1	91.5
-90°	35	80.7	101.1	90.9	153.7	58.3	123.2	142.7	121.4	103.8	85.7	115.2
frequency (Hz)	49	83.9	104.9	107.1	142.8	62.4	137.7	145.1	135.5	90.7	68.5	90.4
Resonant	35	0	0	0.95	1.23	2.11	0.6	0.7	1.0	0.15	0.43	0.14
peak (dB)	49	0	0	0.8	0.7	1.2	0.43	0.45	0.58	0.16	0.23	0.15

The frequency response results for open loop and open loop with hysteresis compensation are presented in Fig. 19 (a) and (b). The hysteresis compensation causes relocation of the starting amplitude to 0 dB as well as starting phase to 0° for both amplitudes. In consequence the bandwidth frequencies are moved from 25 Hz to 40 Hz for -3 dB and 81 Hz to 101 Hz for -90° with a 35 µm reference amplitude.

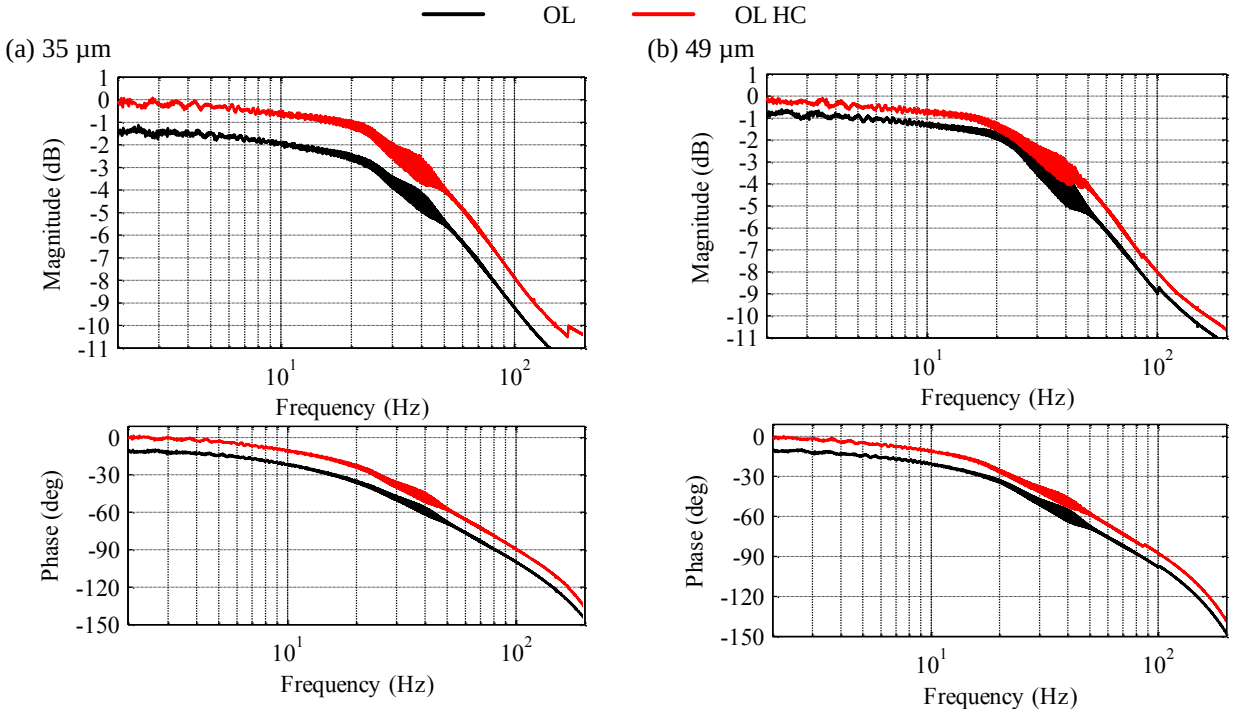

Fig. 19 OL and OL HC frequency response for (a) 35 µm and (b) 49 µm

The frequency response results for closed loop PID control are presented in Fig. 20 (a) and (b). The results show that the PID control improves the frequency response to 165 Hz for -3 dB and 154 Hz for -90° with the PID 2 gains and 35 µm amplitude much higher bandwidths than open loop control, but this controller also gives a resonant peak of 1.23 dB. Note that this set of gains (PID 2) caused power down of the amplifier before 250Hz was reached.

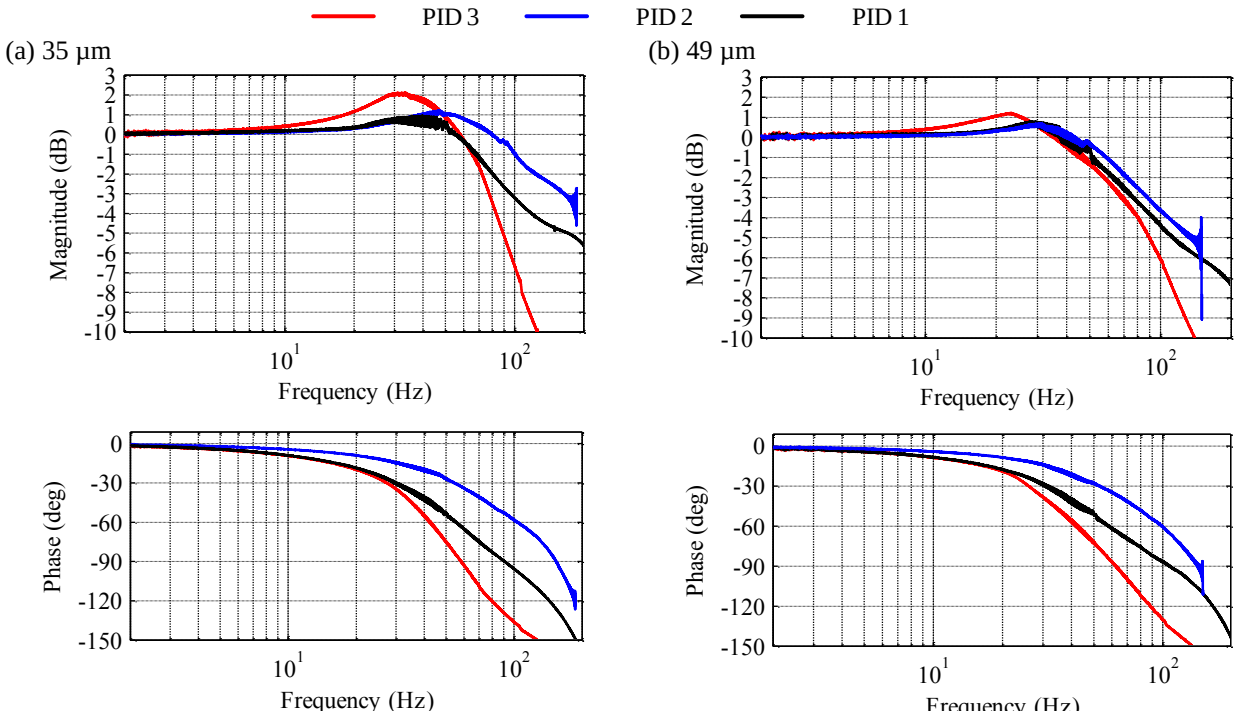

Fig. 20 PID frequency response for (a) 35 µm and (b) 49 µm

The frequency response results for PID HC are presented in Fig. 21 (a) and (b). The maximum -3dB frequency achieved is 124.9 Hz for PID HC 5, but this value was obtained with a lower resonant peak (0.7 dB) than the best PID controller without hysteresis compensation (PID 2). Furthermore, the -90º frequency for the 35 µm amplitude is only lower by 10 Hz and is better for the 49µm amplitude.

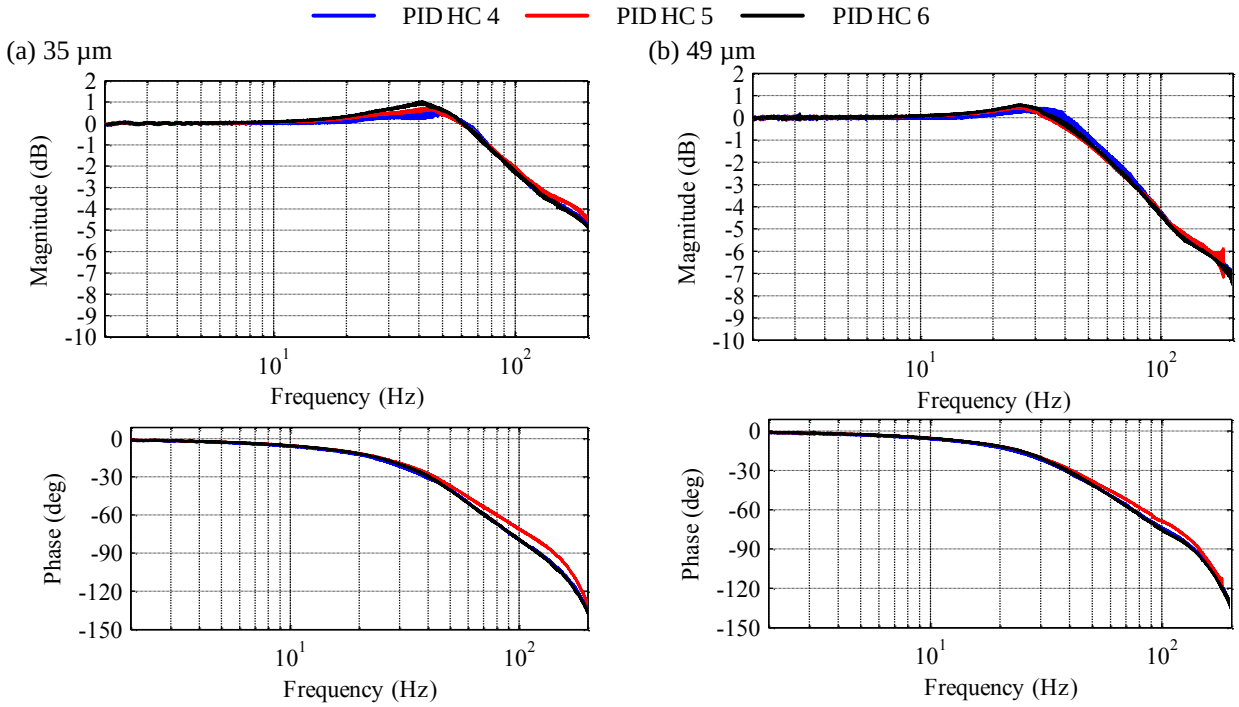

Fig. 21 PID HC frequency response for (a) 35 µm and (b) 49 µm

The frequency response results for the FF PID G controller are presented in Fig. 22 (a) and (b). A common feature is a much lower resonant peak than the other control techniques. Almost 110 Hz (for 35 µm amplitude) for -3 dB frequency

was achieved with FF PP G 6 while the response remains flat. The -90º phase was reached at 115 Hz. This makes the FF PID G controller a good compromise between maximum operation frequency and flat response, compared to other control techniques.

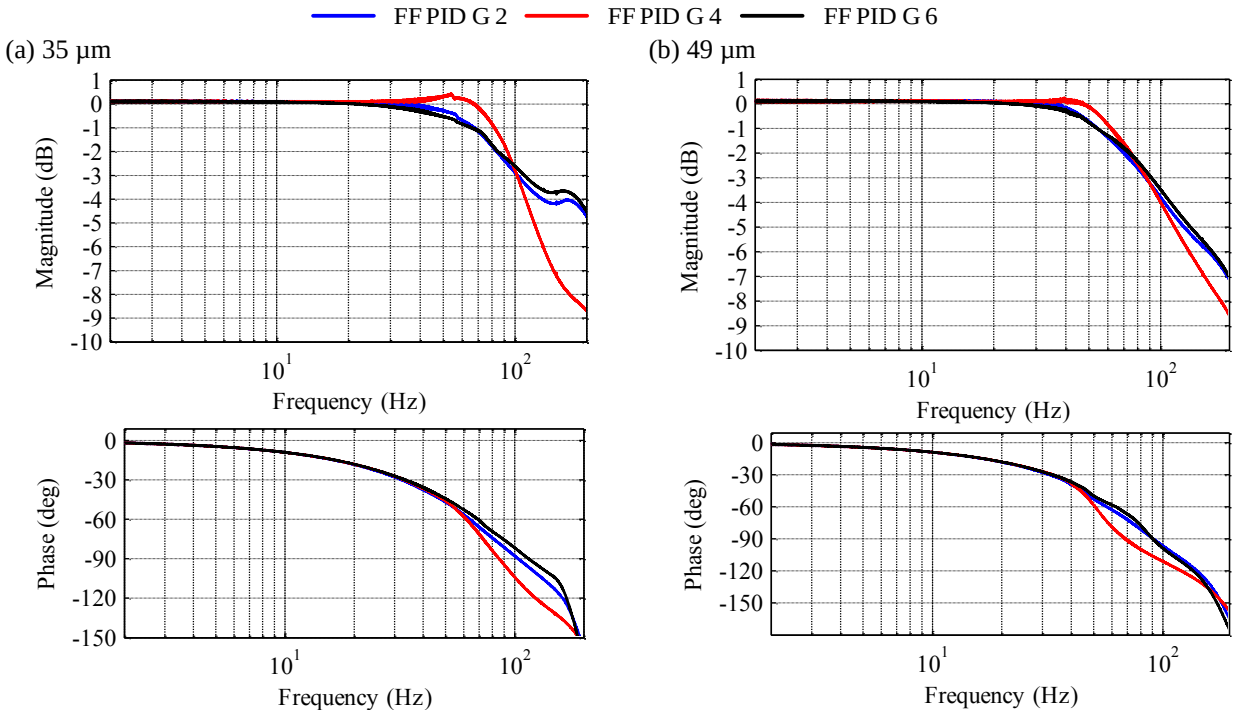

Fig. 22 FF PID G frequency response for (a) 35 µm and (b) 49 µm

6. Conclusions

The control of a new proportional hydraulic valve driven by a piezoelectric ring bender actuator has been investigated in this paper. In particular, the actuator hysteresis problem is addressed; hitherto this has been a major obstacle in the adoption of smart materials for valve actuation.

A Generalized Prandtl-Ishlinskii model has been adapted to represent the hysteretic relationship between the voltage applied to the piezoelectric actuator and the resulting valve spool displacement. Model parameters are estimated by a least-squares fit to experimental data. The hysteresis gives a deviation of 17% of maximum displacement away from the ideal linear relationship. Applying a real-time analytical inverse of the hysteresis model (open loop) linearizes the actuator behaviour very effectively, reducing the error to a maximum of 2.6% and an average of 1.5%. Uncompensated, hysteresis significantly effects steady state accuracy as evident in step response results, and also reduces amplitude ratio by 1.5dB and introduces an extra 10° phase lag in the frequency response results; these effects are eradicated when hysteresis compensation is used. The -90° phase lag frequency, which is the conventional measure of bandwidth used for servovalves and other hydraulic proportional flow control valves, is increased from about 80Hz to 100Hz as a result.

Closed loop position control of a valve spool requires additional position sensing and interfacing hardware, but potentially improves positional accuracy and dynamic response. Conventional PID control has been investigated, and also three PID variants incorporating hysteresis compensation. Increasing the -90° bandwidth frequency to about 150Hz is shown to be realistic. Although similar bandwidths can be achieved with and without hysteresis compensation in the forward path (i.e. comparing PID HC and PID, for example PID HC 5 and PID 2), they can only be achieved without hysteresis compensation if higher controller gains are used which increase the size of the resonant peak and also cause more overshoot in the step response (particularly at low amplitude as in Fig. 17(c)). Hysteresis compensation in a command feedforward path is only satisfactory if a dynamic model (or filter) is included in the command to the feedback loop (the FF PID G controller), or otherwise overshoot is too high. Comparing frequency responses, although the bandwidth achieved with FF PID G is generally lower than PID HC, the response is nearly flat (little or no resonant peak) which may be an advantage in some applications. Overall it may be concluded from the controller tests that:

(i) Open loop hysteresis compensation improves accuracy (significantly) and frequency response
(ii) Conventional closed loop PID control is also effective at overcoming the hysteresis problem, although necessitating position feedback, and avoids the need for hysteresis modelling.

(iii) Closed loop hysteresis compensation schemes, either PID HC or FF PID G, achieve the best performance in terms of high speed of response but without so much overshoot or resonant amplification as with conventional PID.

The spool in the prototype valve is from a commercial Moog E024 series servovalve [46], which has a rated flow of up to 7.5 L/min with 35bar pressure drop across each valve orifice. The valve is designed for a maximum supply pressure of 210bar. In the commercial E024 valve, like most servovalves, the spool is actuated by hydraulic pressure controlled by an electromagnetic torque motor. This actuation mechanism is a complex design requiring highly precise machining, manual assembly, and an accurate calibration process, and thus piezoelectric actuation is an attractive alternative. Conventional valves of this size have -90° bandwidths in the region 50Hz to 300Hz, and thus the prototype valve has a broadly similar dynamic performance, particularly with closed loop control. The E024 like most servovalves is specified to have hysteresis less the 3% [46], and so even without closed loop control the prototype valve can achieve this if hysteresis compensation is implemented using the inverse model.

In summary, the original contributions of this work are:

(i) The implementation of a generalized Prandtl-Ishlinskii model of hysteresis and demonstration that this model can be trained to fit the hysteretic behaviour of piezo-actuated device very well.
(ii) Analytical inversion of the model, and experimental demonstration that this inverse can cancel out the actuator hysteresis very effectively.
(iii) A detailed comparison of closed loop control schemes with and without embedded hysteresis compensation.
(iv) The first in-depth control performance results for a novel piezoelectric ring bender actuated spool valve designed for controlling high pressure hydraulic actuation systems.
(v) Demonstration that resulting valve performance, in terms of hysteresis and dynamic response, is comparable with commercial valves using much more complex pilot stage actuation.

Acknowledgements

This work was funded in part by Innovate UK through the VITAL (Valve Integration Through Additive Layer-manufacturing) project in conjunction with Moog Aircraft Group and Renishaw plc.

7. References

[1] J. Mohd Jani, M. Leary, A. Subic, M.A. Gibson, A review of shape memory alloy research, applications and opportunities, Mater. Des. 56 (2014) 1078–1113.
[2] A. Chaudhuri, N. Wereley, Compact hybrid electrohydraulic actuators using smart materials: A review, J. Intell. Mater. Syst. Struct. 23 (2012) 597–634. doi:10.1177/1045389X11418862.
[3] J. Persson, A. Plummer, C. Bowen, I. Brooks, Design and Modelling of a Novel Servovalve Actuated by a Piezoelectric Ring Bender, in: ASMEBATH 2015 Symp. Fluid Power Motion Control, ASME, Chicago, 2015.
[4] J.E. Lindler, E.H. Anderson, Piezoelectric direct drive servovalve, in: SPIEs 9th Annu. Int. Symp. Smart Struct. Mater., International Society for Optics and Photonics, 2002: pp. 488–496.
[5] J. Jeon, C. Han, J.U. Chung, S.-B. Choi, Performance evaluation of a piezoactuator-based single-stage valve system subjected to high temperature, Smart Mater. Struct. 24 (2015) 015022.
[6] G. Changbin, J. Zongxia, A piezoelectric direct-drive servo valve with a novel multi-body contacting spool-driving mechanism: Design, modelling and experiment, Proc. Inst. Mech. Eng. Part C J. Mech. Eng. Sci. 228 (2014) 169–185.
[7] H. Murrenhoff, High response hydraulic servovalve with piezo-actuators in the pilot stage, Olhydraulik Pneum. (2006) 1–17.
[8] F. Bauer, M. Reichert, The use of piezo-actuators for high dynamic servovalves, Hydraul. Pneum. 49 (2005) 1–16.
[9] M. Samadani, S. Behbahani, C. Nataraj, A reliability-based manufacturing process planning method for the components of a complex mechatronic system, Appl. Math. Model. 37 (2013) 9829–9845.
[10] P. Sente, C. Vloebergh, F. Labrique, P. Alexandre, Control of a direct-drive servo-valve actuated by a linear amplified piezoelectric actuator for aeronautic applications, in: Electr. Mach. 2008 ICEM 2008 18th Int. Conf. On, IEEE, 2008: pp. 1–6.
[11] S. Li, W. Bao, Influence of magnetic fluids on the dynamic characteristics of a hydraulic servo-valve torque motor, Mech. Syst. Signal Process. 22 (2008) 1008–1015.
[12] D.A. Hall, Review nonlinearity in piezoelectric ceramics, J. Mater. Sci. 36 (2001) 4575–4601.
[13] P. Krejci, K. Kuhnen, Inverse control of systems with hysteresis and creep, IEE Proc.-Control Theory Appl. 148 (2001) 185–192.
[14] D. SĘDZIAK, Basic investigations of electrohydraulic servovalve with piezo-bender element, Arch. Technol. Masz. Autom. 26 (2006) 185–190.
[15] A. Milecki, Modelling and investigations of electrohydraulic servo valve with piezo element, Arch. Technol. Masz. Autom. 26 (2006) 177–184.
[16] D. Sędziak, R. Regulski, Design and Investigations into the Piezobender Controlled Servovalve, in: Solid State Phenom., Trans Tech Publ, 2015: pp. 520–525.
[17] S. Karunanidhi, M. Singaperumal, Mathematical modelling and experimental characterization of a high dynamic servo valve integrated with piezoelectric actuator, Proc. Inst. Mech. Eng. Part J. Syst. Control Eng. 224 (2010) 419–435.
[18] D.K. Sangiah, A.R. Plummer, C.R. Bowen, P. Guerrier, A novel piezohydraulic aerospace servovalve. Part 1: design and modelling, Proc. Inst. Mech. Eng. Part J. Syst. Control Eng. 227 (2013) 371–389.
[19] V. Hassani, T. Tjahjowidodo, T.N. Do, A survey on hysteresis modeling, identification and control, Mech. Syst. Signal Process. 49 (2014) 209–233.
[20] F. Preisach, Über die magnetische Nachwirkung, Z. Für Phys. 94 (1935) 277–302.
[21] M.A. Krasnosel'Skii, A.V. Pokrovskii, Systems with hysteresis, Springer Science & Business Media, 2012.
[22] M.-L. Zhou, Y. Tian, W. Gao, Z. Yang, High precise control method for a new type of piezoelectric electro-hydraulic servo valve, J. Cent. South Univ. Technol. 14 (2007) 832–837.
[23] G.-Y. Gu, L.-M. Zhu, C.-Y. Su, H. Ding, S. Fatikow, Modeling and Control of Piezo-Actuated Nanopositioning Stages: A Survey, (2014) 1–20.

[24] H. Hu, R.B. Mrad, A discrete-time compensation algorithm for hysteresis in piezoceramic actuators, Mech. Syst. Signal Process. 18 (2004) 169–185.
[25] L. Riccardi, D. Naso, H. Janocha, B. Turchiano, A precise positioning actuator based on feedback-controlled magnetic shape memory alloys, Mechatronics. 22 (2012) 568–576.
[26] G. Binetti, G. Leonetti, D. Naso, B. Turchiano, Comparison of Model-free and Model-based Control Techniques for a Positioning Actuator based on Magnetic Shape Memory Alloys, in: Mechatron. ICM 2015 IEEE Int. Conf. On, IEEE, 2015: pp. 284–289.
[27] W.J. Thayer, Specification Standards for Electrohydraulic Flow Control Servovalves, Moog Technical Bulletin 117, Moog Inc Control Div. (1962).
[28] M.J.F. Bertin, A.R. Plummer, C.R. Bowen, D.N. Johnston, An Investigation of Piezoelectric Ring Benders and Their Potential for Actuating Servo Valves, in: ASMEBATH 2014 Symp. Fluid Power Motion Control, American Society of Mechanical Engineers, 2014: pp. V001T01A034–V001T01A034.
[29] M. Brokate, J. Sprekels, Hysteresis and Phase Transitions, Springer, New York, 1996.
[30] K. Kuhnen, Modeling, identification and compensation of complex hysteretic nonlinearities: A modified Prandtl-Ishlinskii approach, Eur. J. Control. 9 (2003) 407–418.
[31] L. Riccardi, D. Naso, B. Turchiano, H. Janocha, Design of linear feedback controllers for dynamic systems with hysteresis, Control Syst. Technol. IEEE Trans. On. 22 (2014) 1268–1280.
[32] L. Riccardi, D. Naso, B. Turchiano, H. Janocha, Adaptive control of positioning systems with hysteresis based on magnetic shape memory alloys, Control Syst. Technol. IEEE Trans. On. 21 (2013) 2011–2023.
[33] M. Al Janaideh, S. Rakheja, C.-Y. Su, A generalized Prandtl–Ishlinskii model for characterizing the hysteresis and saturation nonlinearities of smart actuators, Smart Mater. Struct. 18 (2009) 045001.
[34] M. Al Janaideh, S. Rakheja, C.-Y. Su, An analytical generalized Prandtl–Ishlinskii model inversion for hysteresis compensation in micropositioning control, Mechatron. IEEE ASME Trans. On. 16 (2011) 734–744.
[35] M. Al Janaideh, S. Rakheja, C.-Y. Su, Experimental characterization and modeling of rate-dependent hysteresis of a piezoceramic actuator, Mechatronics. 19 (2009) 656–670.
[36] H. Sayyaadi, M.R. Zakerzadeh, Position control of shape memory alloy actuator based on the generalized Prandtl–Ishlinskii inverse model, Mechatronics. 22 (2012) 945–957.
[37] B. Minorowicz, A. Nowak, F. Stefanski, Hysteresis Modelling in Electromechanical Transducer with Magnetic Shape Memory Alloy, Przegląd Elektrotechniczny. 11 (2014) 244–247.
[38] H. Janocha, K. Kuhnen, Real-time compensation of hysteresis and creep in piezoelectric actuators, Sens. Actuators Phys. 79 (2000) 83–89.
[39] A.R. Plummer, Closed-loop velocity control for an electrohydraulic impact test, PTMC 2005. (2005) 75–90.
[40] W.-D. Chang, R.-C. Hwang, J.-G. Hsieh, A multivariable on-line adaptive PID controller using auto-tuning neurons, Eng. Appl. Artif. Intell. 16 (2003) 57–63.
[41] C. Pedret, R. Vilanova, R. Moreno, I. Serra, A refinement procedure for PID controller tuning, Comput. Chem. Eng. 26 (2002) 903–908.
[42] M.E.-S.M. Essa, M.A. Aboelela, M.A.M. Hassan, Position control of hydraulic servo system using proportional-integral-derivative controller tuned by some evolutionary techniques, J. Vib. Control. (2014) 1077546314551445.
[43] PID Tuning Algorithm - MATLAB & Simulink, http://www.mathworks.com/help/slcontrol/ug/pid-tuning-algorithm.html (accessed November 24, 2015).
[44] K.J. Aström, T. Hägglund, Advanced PID control, ISA-The Instrumentation, Systems, and Automation Society; Research Triangle Park, NC 27709, 2006.
[45] D. Marquardt, An Algorithm for Least-Squares Estimation of Nonlinear Parameters, J. Soc. Ind. Appl. Math. 11 (1963) 431–441. doi:10.1137/0111030.
[46] EO24 Datasheet, http://www.moog.com/literature/ICD/e024seriesmicrovalves-ds.pdf (accessed December 15, 2015).